Photoemission from Al(100) and (111): Experiment and *ab initio* theory

E. E. Krasovskii,[1,2] W. Schattke,[1,3] P Jiříček,[4] M. Vondráček,[4] O. V. Krasovska,[2] V. N. Antonov,[2] A. P. Shpak,[2] and I. Bartoš[4]

[1]*Institut für Theoretische Physik und Astrophysik, Universität Kiel, D-24098 Kiel, Germany*
[2]*Institute of Metal Physics, National Academy of Sciences of Ukraine, 03142 Kiev, Ukraine*
[3]*Donostia International Physics Center (DIPC), 20018 Donostia-San Sebastian, Spain*
[4]*Institute of Physics, Academy of Sciences of the Czech Republic, 162 53 Prague, Czech Republic*

(Received 4 July 2008; published 7 October 2008)

Photoelectron spectra from (100) and (111) surfaces of aluminum in the photon energy range 44–100 eV are measured and calculated within an *ab initio* one-step theory. Dispersion of spectral structures is interpreted in terms of unoccupied electronic structure of a semi-infinite crystal. The energy dependence of complex self-energy is derived from the experiment. The lifetimes of the (100) and (111) surface states and the photon energy dependence of the intensity of photoemission from the surface states are determined. A broad spectral structure is experimentally observed at the (111) surface, which disappears at the room temperature. It is tentatively interpreted as a surface resonance.

DOI: 10.1103/PhysRevB.78.165406 PACS number(s): 79.60.−i, 73.20.−r, 61.05.jd, 71.15.Ap

I. INTRODUCTION

Owing to its simplicity aluminum is of fundamental importance for solid-state theory and thus has been a popular object of experimental and *ab initio* studies. Its electronic structure is one of the most accessible computationally, and a quantitative agreement between band-structure calculations and experiment was achieved in late 70's.[1,2] Since then aluminum has served as a textbook example of a nearly-free-electron metal. The one-particle band structure is known to satisfactorily describe the Fermi surface,[1] optical spectrum,[2,3] and plasmon excitations[4] in aluminum.

Electronic structure of low index surfaces of aluminum has been theoretically addressed many times both within a semi-infinite crystal[5–13] and within a supercell slab approach.[14–17] A number of angle-resolved photoemission (ARPES) measurements have been reported,[17–23] however, a consistent theory that would describe the observed energy distribution curves (EDC) including the emission from surface states has not yet been presented. In spite of the simple and well understood band structure of the occupied states, photoemission from aluminum is very challenging for *ab initio* calculations. First, for the free-electron-like initial states, the one-dimensional ($\vec{k}_\parallel$ projected) density-of-states function is rather structureless—in contrast to *d* states, where this function changes rapidly with energy. For aluminum, it is the final states that form the structure of the EDCs. Thus, a detailed knowledge of unoccupied band structure is required to calculate the spectra. Second, the transition probabilities are rather sensitive to inelastic effects (imaginary part of the self-energy), which cannot be reliably calculated by the state-of-the-art methods and have to be inferred from the experiment. Furthermore, the valence band of aluminum is 11 eV wide, so the complex self-energy may considerably change within one spectrum.

The one-step theory of photoemission[24] within a multiple-scattering approach was first applied to Al(100) at photon energies below 30 eV in Ref. 8. Below the plasma frequency $\omega_p = 15$ eV the emission intensity was found to be strongly affected by the screening of the electric field at the surface. For photon energies well above ω_p, the only previous calculation of the EDCs was performed in Ref. 9 within a quasi-one-dimensional model for the crystal potential. It showed general agreement with experimental spectral profiles and correctly gave the resonant photon energy of the surface-state emission. However, it has also revealed limitations of the nearly-free-electron model; the surface-state emission intensity was overestimated by an order of magnitude below the resonance and underestimated at the resonance. The reason for this is, apparently, the averaging of the crystal potential over the (100) lattice planes, which neglects the scattering of the outgoing electron along the surface. It has recently been shown[13] that the multiple scattering (band-structure effects) plays a crucial role in formation of the final states responsible for the enhancement of the surface-state emission.

In this work we present a combined experimental and theoretical study of the normal emission from Al(100) and (111) surfaces with the aim to provide an interpretation of the observed bulk and surface-state photoemission in terms of complex band structure of a semi-infinite crystal.[25] By adjusting the energy dependent self-energy shift and the inelastic-scattering rate (optical potential) we obtain a convincing agreement of the one-step photoemission calculation with the experiment. Still, the uncertainties in the theoretical description of the spectral shape cannot be completely eliminated; we shall show that difficulties arise when the final state comprises several Bloch waves, in which case a detailed knowledge of the self-energy operator is required to correctly describe the photoelectron spectrum.

The paper is organized as follows: after the description of the experimental setup in Sec. II and computational methodology in Sec. III, we discuss the photoelectron spectra from the (100) and (111) surfaces in Secs. IV and V, respectively. Some aspects of inelastic scattering are discussed in Sec. VI.

II. EXPERIMENT

The Al(100) and Al(111) crystals (Surface Preparation Laboratory Zaandam, the Netherlands) with dimensions of

$10\times10\times1$ mm^3 were cut, polished on one side, and oriented with respect to the surface normal to within 0.50°. The cleaning procedure was the same for both crystals; several ion-bombardment-annealing cycles (1000 eV Ar+ ions, 15 μA, 30 min sputtering; 450 °C flash for 10 s) produced atomically clean surface checked by x-ray photoemission and low energy electron diffraction (LEED).

The ARPES measurements were performed at the Elettra synchrotron-radiation source in Trieste at the Material Science Beamline. The ultra high vacuum (UHV) experimental chamber with a base pressure in the 10^{-10} mbar range is equipped with a 150 mm mean radius electron energy analyzer Phoibos 150 (SPECS production) with a multichannel detection. The electron energy analyzer worked in the constant pass energy mode (4 eV). The energy resolution for the monochromator and the electron energy analyzer was 150 meV. The angular resolution was ~2°. The valence-band spectra were collected in normal emission and the radiation was directed at 45° with respect to the surface normal for both crystals.

The EDCs of Al(100) crystal were collected at a temperature about 170 K for the synchrotron-radiation energies from 50 to 100 eV. The temperature of the sample was measured by a thermocouple, type *K*, directly attached to the rear side of the crystal. For Al(111) the photon energy varied from 44 to 75 eV. The spectra for this surface were recorded both at room temperature and at about 165 K.

The background of the EDCs was subtracted by the Shirley procedure. The interfering Auger excitations as well as the signal from the second-order frequency were removed. (Core level excitation cross section taken from Ref. 26.)

The LEED intensity measurement of the specular beam of the Al(111) crystal was performed in the ADES 400 photoelectron spectrometer (VG product) equipped with rear view LEED (SPECS product). For this experiment the same Al(111) sample as for photoemission measurement was used. To visualize the specular beam from the Al(111) crystal surface the sample was slightly deflected (~5°) from the normal direction. The diffraction patterns were measured in 2 eV step in the energy range from 25 to 60 eV, recorded by a charge-coupled device (CCD) video camera and stored into a computer. The energy dependence of the specular beam intensity was obtained from stored LEED patterns using AIDA program (SPECS product). Linear background was subtracted from the specular beam intensities and corrected for the primary electron-beam current.

III. COMPUTATIONAL METHODOLOGY

The *ab initio* calculations of ARPES are performed within the one-step photoemission theory[24] in a semi-infinite crystal geometry using the band-structure approach[27] both to final and to initial states. The crystal potential both at the surface and in the bulk is determined self-consistently within the local-density approximation (LDA) by the augmented Fourier components method.[28] The complex band structure[29] (CBS) is calculated with the inverse $\mathbf{k}\cdot\mathbf{p}$ method[30] in the extended linear augmented plane-wave formalism.[11]

The emission intensity at a photon energy ω is determined by the transition probability between an initial state $|\Psi\rangle$ of energy E_{ini} and the so-called photoemission final state $|\Phi\rangle$. The latter is the time reversed LEED state of energy $E_{\mathrm{fin}}=E_{\mathrm{ini}}+\hbar\omega$. (The LEED wave function is a scattering solution for a plane-wave incident from vacuum.) The inelastic scattering is described by an imaginary part $-iV_i$ (optical potential) added to the potential in the crystal half-space, so that $|\Phi\rangle$ is an eigenfunction of a non-Hermitean Hamiltonian with a real eigenvalue E_{fin}. The term $-iV_i$ governs the spatial decay of the function $|\Phi\rangle$ into bulk, which is responsible for the surface sensitivity of photoemission in the one-step model. In the crystal half-space, where the potential is periodic, the function $|\Phi\rangle$ is given by its partial waves (CBS) expansion: $|\Phi\rangle=\Sigma|\kappa_i\rangle$, each partial wave $|\kappa_i\rangle$ being a Bloch wave that satisfies the Schrödinger equation with a complex surface-normal projection κ_i of the wave vector. In the presence of optical potential, all κ_i have a nonzero imaginary part; the waves that have complex wave vectors also with $V_i=0$ are referred to as genuinely evanescent waves. The initial state is a standing wave; in the depth of the crystal, in the simplest case of aluminum it is a sum of the Bloch wave $|k_+\rangle$ incident from the interior of the crystal on the surface and a reflected wave $|k_-\rangle$. Close to the surface region the decaying part of the CBS contributes to $|\Psi\rangle$, but in the particular case of normal emission from Al its contribution has turned out to be negligible.

In order to establish a connection between the observed spectra and the band structure of aluminum we shall analyze the partial contributions $\langle\Phi|\hat{\mathbf{p}}|k_+\rangle$ and $\langle\Phi|\hat{\mathbf{p}}|k_-\rangle$ to the dipole matrix element $\langle\Phi|\hat{\mathbf{p}}|\Psi\rangle$. The transition amplitudes $\langle\Phi|\hat{\mathbf{p}}|k_\pm\rangle$, in turn, split into contributions from different branches of the unoccupied CBS, which often makes a band mapping analysis too complicated to be performed without a one-step calculation.[31]

The final-state energy dependence of V_i was determined by fitting the calculated width of spectral structures to the experiment and approximated by a parabolic curve in the energy interval 30–100 eV, see Fig. 3 in Sec. IV.

For the initial states the potential is assumed real. The finite hole lifetime is included by a Lorentzian broadening of the spectral function, with the full width at half-maximum (FWHM) growing linearly from 0.3 eV at the Fermi level to 2.5 eV at the bottom of the valence band. The finite-energy resolution was taken into account by the convolution of the theoretical spectrum with a Gaussian of FWHM=0.15 eV. For the surface-state peak it was important to use a photon energy dependent energy resolution, see Sec. IV B. The inverse lifetime of the surface state determined by fitting a Voigt profile to the experimental lineshape is 0.28 eV for the (100) and 1 eV for the (111) surface state.

IV. PHOTOEMISSION FROM Al(100)

First angular resolved ultraviolet photoemission experiments on the Al(100) surface were performed 30 years ago.[19,20] Five years later a detailed synchrotron-radiation study of both valence band and surface-state emission from Al(100) in the range 50–100 eV was reported.[21] In particular, the surface-state emission intensity showed strong enhancement at about $\hbar\omega=73$ eV with a 20 eV wide maximum in

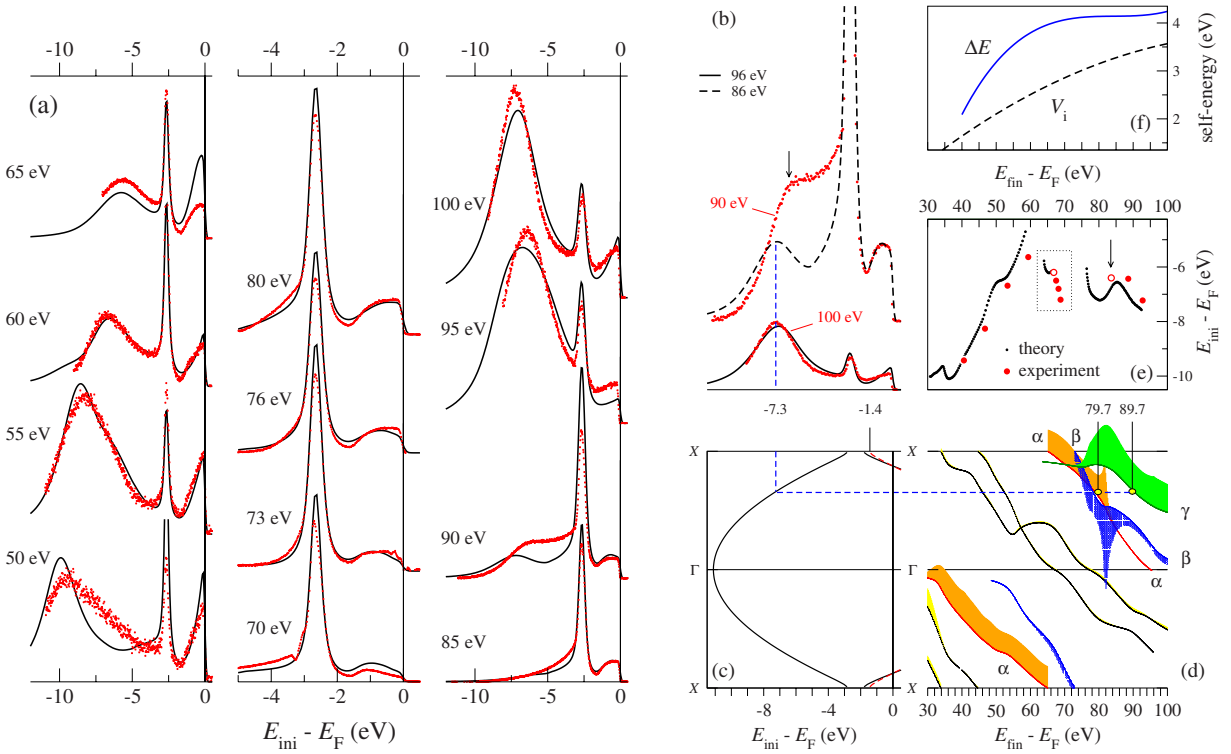

FIG. 1. (Color online) (a) Comparison of theoretical (lines) and measured (dots) EDCs for Al(100). (b) Photoelectron spectra without self-energy correction (lines) for ω=86 and 96 eV compared to measured spectra (dots) for ω=90 and 100 eV, respectively. (c) Occupied band structure of Al along the $X\Gamma X$ line. Corrected dispersion of the second band is shown by a dashed line starting at E_{ini}=−1.4 eV. Straight dashed lines show the location of the initial state at E_{ini}=−7.3 eV and the direct transition to the branches α and γ of the final-states CBS. (d) Energy dependence of the real part of the Bloch vector for most important partial waves in the Bloch wave decomposition of the LEED state. The current carried by individual waves is shown by the vertical extent of the shaded area. (e) Peak dispersion diagram: dependence of the energy location E_{ini} of the EDC peaks (first valence band) on the final-state energy E_{fin} by the *ab initio* calculation (dots) and from the experiment (circles). Well defined maxima are shown by full circles and the two shoulders by open circles. (f) Energy dependence of the optical potential V_i (dashed line) and the self-energy shift ΔE (full line) used to obtain the spectra in graph (a).

the constant initial-state (CIS) spectrum. The peak positions in the energy distribution curves and the photon energy dependence of the emission intensities were found consistent with a nearly-free-electron picture.

Surprisingly, in spite of the increasing mean-free path at high energies, the surface-state peak has been recently observed to be the strongest feature also at high energies (125–760 eV).[23] Furthermore, contrary to the expectation, the intensity of the surface-state peak relative to the bulk emission is increased with increasing both photon energy and temperature. To explain the temperature dependence the authors of Ref. 23 assumed different role of atomic vibrations in the bulk and at the surface and related the photon energy dependence to the increasing role of the Debye-Waller factor with increasing energy.

In view of this observation, it is important to establish whether the optical potential description of inelastic scattering yields the correct relative intensities between the surface state and the bulk emission.

A. Energy distribution curves

Measured and calculated photoelectron spectra for photon energies 50–100 eV are presented in Fig. 1(a). They show a nondispersive peak at −2.65 eV due to the surface state at the point X in the Brillouin zone and a strongly dispersive maximum below the surface-state peak (first valence band). At first glance the dispersion of the maximum is consistent with a nearly-free-electron (NFE) structure of final states, but the strongly non-Lorentzian shapes of the experimental maxima suggest that the spectra cannot be understood in terms of lifetime-broadened direct transitions.

We shall now analyze the spectra in terms of transitions between Bloch constituents of initial and final states. The *ab initio* band structure (without a self-energy correction) is shown in Figs. 1(c) and 1(d). The dependence of the energy location E_{ini} of the spectral maxima on the final-state energy $E_{ini}+\omega$ is referred to as the peak dispersion diagram. The comparison of the calculated diagram to the experiment, Fig. 1(e), clearly demonstrates a self-energy shift of the spectral structures to higher final-state energies; for example the spectrum measured at ω=100 eV coincides with the *ab initio* spectrum for ω=96 eV, see Fig. 1(b). To correct this drawback of the LDA we introduce a transformation of final-state energies $E_{fin}\rightarrow E_{fin}+\Delta E(E_{fin})$. The function $\Delta E(E_{fin})$ that yields the best agreement between theoretical and experimental spectral shapes over the available photon energy range is shown in Fig. 1(f) together with the energy dependence of optical potential.

The width of the gap at the point X is known to be underestimated in the LDA calculations.[13] In order to reproduce the minimum in the EDCs at −1.6 eV we renormalized the dispersion of the second valence band as shown in Fig. 1(c); a linear transformation that leaves the Fermi vector unchanged and brings the point X_1 (bottom of the band) to −1.4 eV gives the best agreement with experiment. Earlier experimental data placed the bottom of the band at −1.15 eV.[21]

The resulting spectra are compared with the experiment in Fig. 1(a). The theory reproduces well the dispersion of the maxima and almost everywhere the lineshape. The most pronounced discrepancy appears at ω=85 and 90 eV; the theoretically predicted maximum does not appear at 85 eV, and at 90 eV it comes out as a shoulder at −6.5 eV [vertical arrows in Figs. 1(b) and 1(e)] instead of −7.3 eV in the theory. Figure 1(d) explains the origin of the difficulty. It shows the CBS branches that effect the photoelectron escape into vacuum; the vertical extent of the shaded area is proportional to the partial current carried by the individual partial wave $|\kappa_i\rangle$ in the CBS decomposition of the LEED state.[32] The ω =100 eV spectrum is due to transitions to the branch γ, whereas around ω=90 eV branches α and β equally strongly contribute to the current. Because the transition amplitudes to different branches interfere the spectral shape becomes very sensitive to the relative positions of the bands. In this case the theory suffers particularly strongly from the uncertainty in self-energy corrections because the assumption of a spatially constant self-energy may fail; owing to the spatial structure of the self-energy operator, different branches should, in principle, be ascribed different values of ΔE and V_i. Evidence of the deficiency of a spatially constant self-energy approximation has been recently presented for a layered crystal $TiTe_2$.[33]

The initial states around −6.5 eV manifest themselves also between ω=72 and 76 eV, see Fig. 2(a); the broad maxima with a downward dispersion [box in Fig. 1(e)] are due to transitions into the branch α around the point X (E_{fin}=65 eV in the LDA calculation). The agreement with experiment in this region is satisfactory, especially in view of the Auger emission due to the hole in the $2p$ core level, which contaminates the experimental spectra.

Figure 2(c) shows the CBS decomposition of the emission intensity for the initial state at −6.15 eV (the shaded area now shows the CBS resolved transition intensities). The comparison with Fig. 1(d) illustrates the selective role of the dipole matrix element. A question often raised is the role of direct and indirect transitions in formation of photoelectron spectra. In the Bloch waves approach the answer is immediately given by the CBS decomposition of the transition intensity from the initial state constituents $|k_-\rangle$ and $|k_+\rangle$ taken separately, see Figs. 2(d) and 2(e). The maxima in the α branch at 56 and 75 eV are seen to come from the direct transitions from $|k_+\rangle$ and $|k_-\rangle$, respectively, whereas β and γ do not show sharp maxima at k_+ or k_-. Around 65 eV the transitions to α are indirect, and the contributions of the two Bloch waves are comparable, which leads to the interference between the transition amplitudes from $|k_-\rangle$ and $|k_+\rangle$,[31] see Fig. 2(f). The spectra are especially sensitive to details of unoccupied band structure when the interference is destructive, as in the interval E_{fin}=72–85 eV. The transitions from the states between −6 and −7 eV to this complicated region correspond to the experimental photon energy range of ω =81–95 eV, which is a possible explanation of the discrepancies in the 85 and 90 eV spectra in Fig. 1(a).

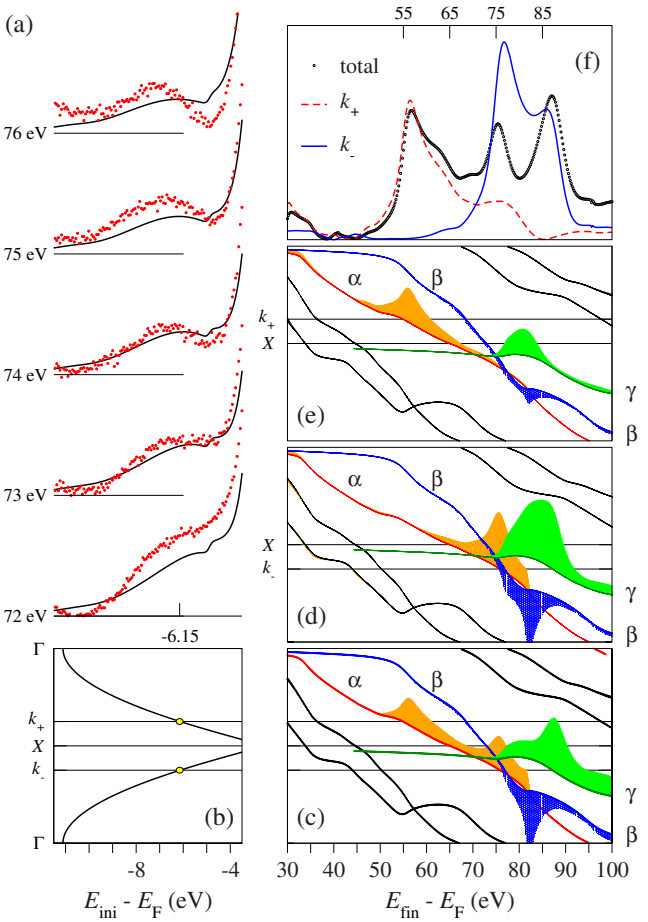

FIG. 2. (Color online) (a) Comparison of the measured and calculated EDCs over the binding-energy region of the first valence band for photon energies 72–76 eV. (b) Energy band structure $E(k_\perp)$ of the first valence band in the (100) direction. k_+ and k_- are the Bloch vectors of the propagating constituents of the initial state at E_{ini}=−6.15 eV. (c) Final-state CBS decomposition of the emission intensity from this initial state. Final-state CBS decompositions of the emission intensity from the $|k_-\rangle$ and $|k_+\rangle$ constituents of the initial state are shown in graphs (d) and (e), respectively. (f) Initial-Bloch-waves resolved intensity distribution: $|\langle\Phi|\hat{\mathbf{p}}|k_+\rangle|^2$ (dashed line), $|\langle\Phi|\hat{\mathbf{p}}|k_-\rangle|^2$ (solid line), and the full CIS spectrum (dotted line).

B. Surface-state emission

The intensity of the surface-state emission cannot be determined by simply measuring the maximum intensity for two reasons. First, as a result of the lifetime broadening, the surface-state peak strongly overlaps with the bulk band emission, so the latter must be subtracted. Second, the width of the surface-state peak grows with photon energy due to the decreasing energy resolution and to the growing effect of the finite angular resolution. The surface-state peak is much

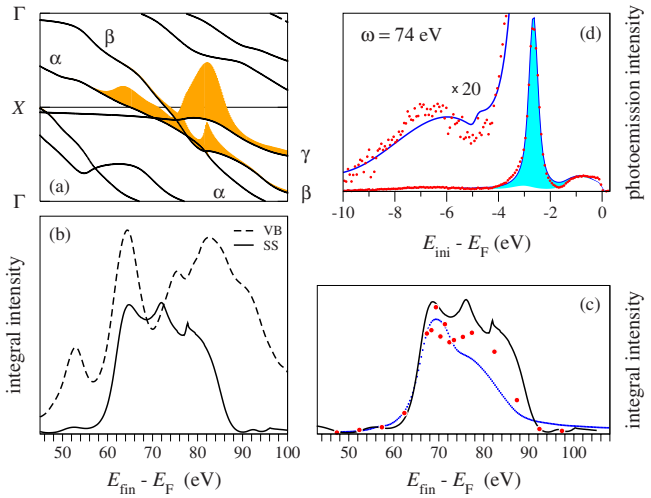

FIG. 3. (Color online) (a) CBS decomposition of the surface-state emission intensity. (b) Dependence of the surface-state emission intensity (solid line) and the bulk valence-band integral intensity (dashed line) on the final-state energy $I(E_{\mathrm{fin}})$. (c) Comparison of the self-energy corrected $I(E_{\mathrm{fin}})$ curve (solid line) with the measurement of the present work (circles) and of Ref. 21 (dotted line). (d) Comparison of the self-energy corrected theoretical EDC for $\omega = 74$ eV (solid line) with the experiment (dots). Shaded area shows the contribution from the surface state.

more affected by the extrinsic broadening than the bulk band emission.

We use the following procedure to avoid these factors: we fit the experimental spectrum with a sum of two curves; the theoretical EDC [with the surface-state contribution subtracted, see Fig. 3(d)] and a Voigt curve. The latter is a convolution of a Lorentzian (constant FWHM of 0.28 eV representing the lifetime broadening) with a Gaussian of a photon energy dependent FWHM. The latter was determined to grow from 0.15 eV at $\hbar\omega=50$ eV to 0.45 eV at 100 eV. The least-squares fitting then yields a coefficient of the Voigt profile, which is the surface-state intensity.

Calculated absolute intensities of the surface state and bulk emission are shown in Fig. 3(b) as solid and dashed curve, respectively. They both are seen to vary strongly with photon energy, especially the surface-state intensity, which grows by more than an order of magnitude over the region from $\hbar\omega=60$ to 70 eV. The experimental surface-state intensity obtained with the procedure described above is shown by circles in Fig. 3(c). It agrees well with the results of Ref. 21 [dotted line in Fig. 3(c)]. However, our measured curve is about 3 eV wider at half-maximum, and it decreases faster at high energies, which is in better agreement with the calculations, solid line in Fig. 3(c). Still, our theory predicts a much steeper intensity decrease at the high energy side than in the experiment.

Note that the surface-state emission is determined by the same three CBS branches; the steep growth at $E_{\mathrm{fin}}=65$ eV is due to direct transitions to the branch α, and at higher energies it is indirect transitions to genuinely evanescent states. This complicated structure leads to a pronouncedly non-Lorentzian CIS curve. The CBS decomposition of the matrix element in Fig. 3(a) refers to the structure of the LEED state in the depth of the crystal and does not include the contribution from the close vicinity of the surface. The latter is of the same order as the contribution from the bulk, but the overall shape of the CIS profile is seen to be determined by the complex band structure.

V. PHOTOEMISSION FROM Al(111)

The surface state at the center of the (111) Brillouin zone was first observed by Kevan *et al.*[18] within a narrow interval of photon energies (emission window) around 53 eV. An attempt to explain the width of this interval in terms of direct transitions within an NFE model has, however, lead to a strongly overestimated photoelectron inverse lifetime, $\Gamma = 4.5$ eV.[18] We shall show that for Al(111) inelastic scattering is much weaker, and that the width of the window is determined by elastic scattering.

A. Energy distribution curves

Our calculated and experimental normal-emission EDCs are compared in Fig. 4. They are in general agreement with those of Ref. 18. For the sake of consistency, in the calculation we have used the same energy dependence of the self-energy shift ΔE and optical potential V_i as for Al(100), see Fig. 1(f). The theoretical spectra are in excellent agreement with the measurements performed at room temperature, Fig. 4(a), whereas, surprisingly enough, at the temperature of 165 K the agreement is less favorable; the low-temperature spectra show a nondispersive structure around −7.5 eV [indicated by arrows in Fig. 4(b)] which has no counterpart in the calculated EDCs and disappears at room temperature (except for $\hbar\omega=60$ eV). Its origin is unclear. The experimental procedure makes the possibility of contamination highly unlikely. One may suppose that we encounter here a surface resonance, which is not reproduced in the calculation (possibly because of the deficiency of the LDA) and which is destroyed at higher temperatures by the atomic vibrations at the surface.

The dispersion of the occupied states in the (111) direction is practically free-electron-like, see right panel of Fig. 5; the parabolic band is split by a narrow 0.25 eV wide gap at the point L at 4.5 eV below the Fermi level. Some of the observed features fit into the picture of direct transitions; with photon energy increase from 44 to approximately 56 eV the peak at −7.5 eV disperses upward across the gap to $E_{\mathrm{ini}}-E_F=-2$ eV. This peak is due to transitions to the CBS branch β, see notation in Fig. 5(c). However, at final-state energies around 60 eV the genuinely evanescent fragment of the branch γ comes into play [here $E_\gamma(\mathrm{Re}\, k_\perp)$ makes a zigzag, see right panel of Fig. 5], and indirect transitions to both β and γ become important. Above $E_{\mathrm{fin}}=65$ eV the branch δ dominates.

At the photon energies 44–49 eV a peak in the second valence band (above the gap) is observed, which disperses downward with increasing photon energy. This feature is due to indirect transitions to the branch β, and it is, thus, very sensitive to the treatment of inelastic scattering in the calculation. This is, apparently, the reason why the spectral shape

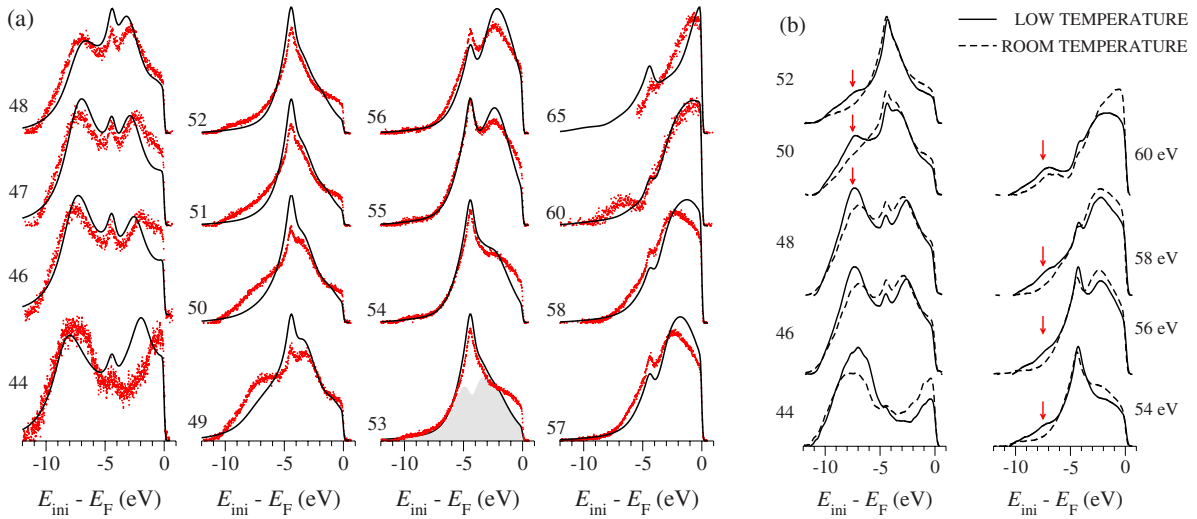

FIG. 4. (Color online) Normal-emission EDCs for Al(111). (a) Theoretical spectra (lines) and room-temperature measurements (dots) for photon energies 44–65 eV. The shaded area in the $\hbar\omega$=53 eV graph shows the contribution from the bulk bands. (b) Comparison of EDCs measured at low (full lines) and room temperature (dashed lines) for photon energies 44–60 eV.

is not perfectly reproduced at $\hbar\omega$=44–47 eV.

B. Surface-state emission

The inverse lifetime of the surface state was determined to be 1 eV by fitting to the experimental lineshapes. The surface-state emission intensity does not contain any adjustable parameters, its energy dependence is shown in Fig. 5(a). The calculated maximum of the surface-state cross section occurs at the final-state energy E_{fin}=45 eV, see Fig. 5. This should be corrected for the self-energy shift of 2.5–3.0 eV, see Fig. 1(f). The FWHM of the $I_{SS}(\omega)$ curve is about 7 eV,

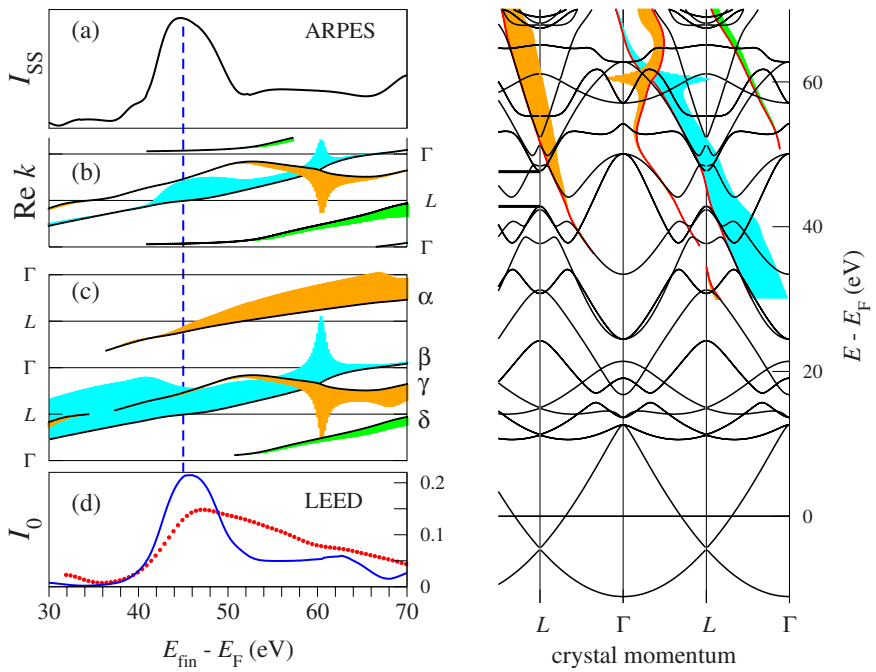

FIG. 5. (Color online) Left panel: (a) Calculated photon energy dependence of the normal emission from the Al(111) surface state, $E_{fin}=E_{SS}-\hbar\omega$. No self-energy correction is introduced. The function $V_i(E)$ is the same as for Al(100), see Fig. 1(f). (b) Partial wave decomposition of the transition probability from the surface state. Vertical extent of the shaded area is proportional to the squared modulus of the momentum matrix element between the surface state and the Bloch wave. (c) Partial wave decomposition of the transmitted current in the LEED calculation, see caption of Fig. 1(d). (d) Experimental (dots) and theoretical (line) intensity of the specularly reflected LEED beam. I_0 is the ratio of the current carried by the normally reflected beam to the incident current. The same LEED states are used to calculate the CIS in graph (a). Experimental spectrum is scaled. Right panel: real band structure in the (111) direction superimposed on the conducting CBS, the same as in graph (c).

which is considerably larger than the value of 4.5 eV obtained in Ref. 18. The disagreement is explained by the fact that even at the maximum the surface-state intensity is much smaller than the integral bulk band intensity, and the latter strongly contributes to the EDC peak, see the $\hbar\omega=53$ eV graph in Fig. 4(a).

The smaller relative intensity of the surface-state emission compared to the (100) case, see Fig. 3(d), stems from a weaker localization of the (111) state, which in turn is a consequence of a smaller gap in which it is located. The decay length is $(\mathrm{Im}\ k)^{-1}=77$ Å for the (111) state and 28 Å for the (100) one. Because the depth sampled by photoemission is much smaller (see Sec. VI) the integral probability of finding the surface state in this region is smaller for the more extended surface state, which leads to a smaller excitation probability.

The surface-state emission increases when the real part of the final-state Bloch vector approaches point L, see Fig. 5. In the absence of the absorbing potential, $V_i=0$, the conducting branch terminates at the Brillouin-zone boundary, and a 4.85 eV wide gap opens in the spectrum of propagating waves (the two ticks at the left border of the right panel of Fig. 5). Within the gap the real part of the Bloch vector stays at L, and the imaginary part forms a "loop" bridging the gap.[29] This gap causes the electron reflection maximum in Fig. 5(d) as well as the enhancement of the surface-state emission in Fig. 5(a). Our LEED measurement of the specularly reflected beam intensity confirms the theoretical prediction that the enhancement of the normal emission from the Al(111) surface state is accompanied by a decrease in the electron transmission at the final-state energy, see Fig. 5(d). The unoccupied conducting CBS in the presence of absorbing potential is shown in Fig. 5(c). Below 45 eV a single CBS branch strongly dominates, as one would expect of a free-electron-like metal, whereas at higher energies two and sometimes three Bloch waves participate in transmitting the incident current into the bulk of the crystal. The energy dependent redistribution of the current among several waves causes an asymmetric shape of the $I_0(E)$ curve, which is confirmed by the experiment.

VI. MEAN FREE PATH

Energy dependence of the photoelectron mean-free path (MFP) and surface sensitivity of photoemission and LEED experiments is traditionally interpreted with the universal U-shaped curve.[34] Limitations of this simple approach have recently become clear. In Ref. 23 the effect of atomic vibrations on the surface sensitivity at high energies was observed. On a smaller energy scale the elastic contribution to the mean-free path was revealed for graphite.[35] The state-of-the-art theoretical determination of λ requires a scattering calculation in the presence of the absorbing potential V_i. It is technically impossible to calculate the function $V_i(E)$ from first principles, so in Ref. 35 it was derived from the shape of the experimental electron transmission spectrum. In the present work the function has been derived from the photoemission experiment by fitting the (100) theoretical EDCs to the measured ones. The same function, dashed curve in Fig. 1(f), highly satisfactory describes EDCs over a wide energy region both for (100) and (111) surfaces. With this function we calculate the energy dependence of the decay factor Im k for the partial waves responsible for the photocurrent. Their decay length $(2\ \mathrm{Im}\ k)^{-1}$ as a function of energy is shown in Fig. 6.

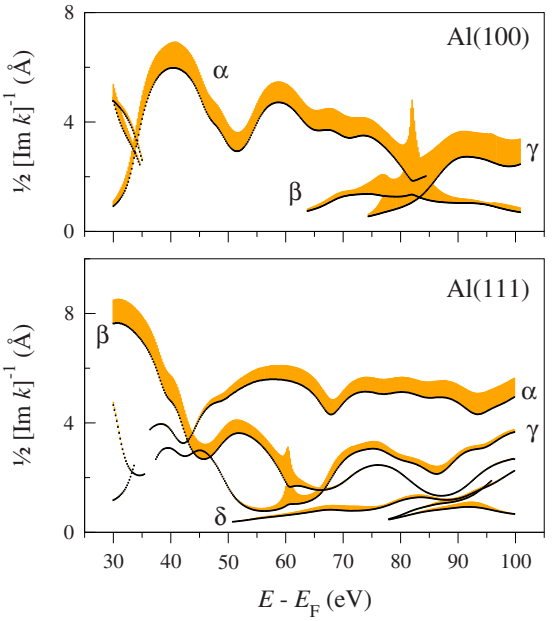

FIG. 6. (Color online) Energy dependence of the penetration depth of most important partial waves in the CBS decomposition of the normal-incidence LEED states for (100) and (111) surfaces of Al. The vertical thickness gives the partial current. The CBS branches are labeled according to Fig. 1(d) and Fig. 5(c) for (100) and (111), respectively.

The MFP λ is associated with the most slowly decaying wave, largest $(\mathrm{Im}\ k)^{-1}$. For example, the center of the (111) emission window corresponds to a minimum of the branch β at 45 eV. The electron MFP at this energy is caused by the reflection from the crystal lattice, and it does not strongly depend on the photoelectron lifetime; for $V_i=2$ eV it is $\lambda=2.7$ Å, and with $V_i=0.5$ eV it is only slightly larger, $\lambda=3.1$ Å.

As a result of the elastic scattering the calculated function strongly deviates from the U curve, in particular, neither for (100) nor for (111) we observe a steady growth of λ above 50 eV. Such behavior is not specific to aluminum; we have observed strong band-structure effects on MFP in layered crystals, $TiTe_2$ (Ref. 33) and graphite.[35] The presence of several branches complicates the picture, so one must be careful in applying these results to interpreting ARPES. For example, the branch α in the (111) case is seen to carry the largest current above 50 eV, but its contribution to photoemission (in the photon energy range studied) is negligible because the momentum matrix elements for both the surface state and the bulk band emission are very small.

VII. CONCLUSIONS

In the present study the major technical difficulties in the description of the electron scattering by the surfaces of alu-

minum have been eliminated. This has made it possible to apply the one-step theory of photoemission with minimal computational uncertainty and to achieve a very convincing agreement with the high-resolution normal-emission measurements for the (100) and (111) surfaces. The close agreement between the calculated and experimental EDCs has enabled us to determine from the experiment the parameters that cannot be calculated from first principles at the present level of computational capabilities; we have determined the energy dependent value of the absorbing potential and the self-energy shift of the quasiparticle final states.

The accurate account of band-structure effects has been instrumental in reproducing the experimentally observed lineshapes and extracting the lifetimes of the surface states. The calculated photon energy dependent ratio between surface-state and bulk band emissions is in good agreement with the experiment for both surfaces. In the energy region studied we do not observe any peculiarities of the surface sensitivity of photoemission; the experimental spectra are well reproduced within the traditional one-step theory, assuming the growth of the optical potential with energy. The absolute values of V_i are of the expected order of magnitude.[31,35]

Elastic scattering of outgoing electrons plays a crucial role in the resonant enhancement of the surface-state emission. In particular, for Al(111) it is purely band-gap emission, which is confirmed by the measurement of electron reflection from the surface.

The role of indirect transitions has been found very important in photoemission from Al(100) and (111), especially when the quantum interference between the Bloch constituents of the initial state becomes strong. Certain difficulties in reproducing the EDC profile at particular energies have been ascribed to the approximation of a spatially uniform optical potential, whose drawbacks may become especially important when the final state is composed of several Bloch waves. The above factors, if not allowed for, may lead to incorrect conclusions in a simple ("geometric") band mapping procedure.

A broad nondispersive structure is experimentally observed in the (111) EDCs, which disappears at the room temperature. It is interpreted as a surface resonance.

Large deviations of the electron mean-free path from the simple *U*-shaped curve have been found and interpreted in terms of the complex band structure in the presence of the absorbing potential.

ACKNOWLEDGMENTS

This work was supported by Science and Technology Center in Ukraine (STCU), Project No. 4930. Support by the Grant Agency of the Czech Republic (Grant No. 202/07/0601), Grant Agency of the Academy of Sciences of the Czech Republic (Grant No. IAA100100628) and by the Institutional Research Plan Grant No. AVOZ 10100521 are gratefully acknowledged by P.J. and I.B. The experimental part was supported by the EU Proj. No. RII3-CT2004-506008.

[1] S. P. Singhal and J. Callaway, Phys. Rev. B **16**, 1744 (1977).
[2] F. Szmulowicz and B. Segall, Phys. Rev. B **24**, 892 (1981).
[3] E. G. Maksimov, I. I. Mazin, S. N. Rashkeev, and Yu. A. Uspenski, J. Phys. F: Met. Phys. **18**, 833 (1988).
[4] K.-H. Lee and K. J. Chang, Phys. Rev. B **49**, 2362 (1994).
[5] D. Spanjaard, D. W. Jepsen, and P. M. Marcus, Phys. Rev. B **19**, 642 (1979).
[6] G. Wachutka, Phys. Rev. B **34**, 8512 (1986).
[7] J. E. Inglesfield and G. A. Benesh, Phys. Rev. B **37**, 6682 (1988).
[8] N. Barberan and J. E. Inglesfield, J. Phys. C **14**, 3114 (1981).
[9] S. K. Ma and Kenneth W.-K. Shung, Phys. Rev. B **49**, 10617 (1994).
[10] W. Hummel and H. Bross, Phys. Rev. B **58**, 1620 (1998).
[11] E. E. Krasovskii and W. Schattke, Phys. Rev. B **56**, 12874 (1997).
[12] E. E. Krasovskii and W. Schattke, Phys. Rev. B **59**, R15609 (1999).
[13] E. E. Krasovskii and W. Schattke, Phys. Rev. Lett. **93**, 027601 (2004).
[14] Ed. Caruthers, L. Kleinman, and G. P. Alldredge, Phys. Rev. B **8**, 4570 (1973).
[15] H. Krakauer, M. Posternak, and A. J. Freeman, Phys. Rev. Lett. **41**, 1072 (1978).
[16] E. V. Chulkov and V. M. Silkin, Surf. Sci. **215**, 385 (1989).
[17] M. J. G. Lee, M. Gensch, A. I. Shkrebtii, Th. Herrmann, W. Richter, N. Esser, and Ph. Hofmann, Phys. Rev. B **72**, 085408 (2005).
[18] S. D. Kevan, N. G. Stoffel, and N. V. Smith, Phys. Rev. B **31**, 1788 (1985).
[19] G. V. Hansson and S. A. Flodström, Phys. Rev. B **18**, 1562 (1978).
[20] P. O. Gartland and B. J. Slagsvold, Solid State Commun. **25**, 489 (1978).
[21] H. J. Levinson, F. Greuter, and E. W. Plummer, Phys. Rev. B **27**, 727 (1983).
[22] C. Sondergaard, P. Hofmann, C. Schultz, M. S. Moreno, J. E. Gayone, M. A. Vicente Alvarez, G. Zampieri, S. Lizzit, and A. Baraldi, Phys. Rev. B **63**, 233102 (2001).
[23] Ph. Hofmann, Ch. Sondergaard, S. Agergaard, S. V. Hoffmann, J. E. Gayone, G. Zampieri, S. Lizzit, and A. Baraldi, Phys. Rev. B **66**, 245422 (2002).
[24] P. J. Feibelman and D. E. Eastman, Phys. Rev. B **10**, 4932 (1974).
[25] Preliminary results of this work have been published in E. E. Krasovskii, W. Schattke, P. Jiříček, V. Dudr, and I. Bartoš, Surf. Sci. **601**, 4105 (2007); E. E. Krasovskii, W. Schattke, P. Jiříček, M. Vondráček, O. V. Krasovska, and I. Bartoš, J. Phys.: Conf. Ser. **100**, 072035 (2008).
[26] R. Haensel, G. Keitel, B. Sonntag, C. Kunz, and P. Schreiber, Phys. Status Solidi A **2**, 85 (1970).
[27] E. E. Krasovskii, Phys. Rev. B **70**, 245322 (2004).

[28] E. E. Krasovskii, F. Starrost, and W. Schattke, Phys. Rev. B **59**, 10504 (1999).
[29] V. Heine, Proc. Phys. Soc. London **81**, 300 (1963); Surf. Sci. **2**, 1 (1964).
[30] I. Bartoš and J. Nadrchal, Surf. Sci. **22**, 290 (1970).
[31] E. E. Krasovskii, V. N. Strocov, N. Barrett, H. Berger, W. Schattke, and R. Claessen, Phys. Rev. B **75**, 045432 (2007).
[32] The concept of partial absorbed currents was introduced in V. N. Strocov, H. I. Starnberg, and P. O. Nilsson, Phys. Rev. B **56**, 1717 (1997), and a detailed explanation has been presented in Ref 35.
[33] E. E. Krasovskii, K. Rossnagel, A. Fedorov, W. Schattke, and L. Kipp, Phys. Rev. Lett. **98**, 217604 (2007).
[34] M. A. Van Hove, W. H. Weinberg, and C.-M. Chan, *Low-Energy Electron Diffraction*, Springer Series in Surface Sciences Vol. 6 (Springer, New York, 1986).
[35] N. Barrett, E. E. Krasovskii, J.-M. Themlin, and V. N. Strocov, Phys. Rev. B **71**, 035427 (2005).